Journal of Applied Physics

A non-linear elastic approach to study the effect of ambient humidity on sandstone

Cite as: J. Appl. Phys. **128**, 244902 (2020); https://doi.org/10.1063/5.0025936
Submitted: 20 August 2020 . Accepted: 06 December 2020 . Published Online: 22 December 2020

Somayeh Khajehpour Tadavani, Kristin M. Poduska, Alison E. Malcolm, and Andrey Melnikov

AIP Publishing

Journal of Applied Physics ARTICLE scitation.org/journal/jap

A non-linear elastic approach to study the effect of ambient humidity on sandstone

Cite as: J. Appl. Phys. **128**, 244902 (2020); doi: 10.1063/5.0025936
Submitted: 20 August 2020 · Accepted: 6 December 2020 ·
Published Online: 22 December 2020

Somayeh Khajehpour Tadavani,[1,a)] Kristin M. Poduska,[1] Alison E. Malcolm,[2,a)] and Andrey Melnikov[2]

AFFILIATIONS

[1]Department of Physics and Physical Oceanography, Memorial University, St. John's A1B 3X7, Newfoundland and Labrador, Canada
[2]Department of Earth Sciences, Memorial University, St. John's A1B 3X5, Newfoundland and Labrador, Canada

[a)]**Authors to whom correspondence should be addressed:** skt660@mun.ca and amalcolm@mun.ca

ABSTRACT

We demonstrate that strong elastic pump wave pulses soften sandstone more in humidified conditions than they do in dry conditions and that this effect is repeatable and reversible. We assess these changes via the non-linear interactions of a strong pump wave with a weaker probe wave. We find that there is an exponential time constant ($\tau \approx 13$ days) associated with this process that is independent of the amplitudes of the pump and the probe, the phase delay between the two waves (the time between transmission of the pump and probe waves), the sampling rate, and whether the sample is being dried or humidified. We demonstrate that the humidity-dependent differences in the amount of softening are induced by only a very small amount of absorbed water vapor and argue that this water is intercalated within clay particles. We also show that our pump–probe experiments detect these humidity-dependent differences in the amount of softening easily and repeatably using an experimental design that does not rely on resonance conditions. This means that, in principle, our experiments could be more easily generalized to other experimental geometries to investigate non-linear elastic properties in complex or irregular sample geometries. Our method and findings have potential relevance in oil and gas exploration, civil engineering, and understanding of the mechanism of earthquakes.

I. INTRODUCTION

Non-linear mesoscopic elastic materials, such as rocks and damaged solids (like steel and plastic), have complex behaviors that are important in applications such as oil and gas exploration, post-seismic recovery processes, and infrastructure integrity monitoring.[1,2] Sedimentary rocks are typically porous and inhomogeneous, made of aggregated rigid grains that have characteristic lengths ranging from tens to hundreds of micrometers. The connections between these grains can function as elastic elements that are heterogeneous in shape and size (on the order of 1 μm) and that constitute less than a few percent of the rock's volume.[1,3] As a result of this network of connections, rocks possess diverse and unique non-linear elastic properties including hysteresis with end-point memory of the previous maximum strain state,[4,5] slow-relaxation phenomena,[6–9] variation of resonance frequency with strain,[2,10,11] and a strong dependence of elasticity on pressure.[12–15] The non-linear properties of a rock can also change when its pore space is saturated with liquid[16–18] or when the humidity of the environment around the rock changes.[19–21] The latter scenario is the focus of this work.

Rocks are complex composite materials, and the interactions between their solid components and any trapped water are surprisingly nuanced. The effect of humidity on linear elastic properties of rocks has been studied by others.[22–25] In this work, we focus on the non-linear interaction of elastic waves in rocks, which continues to be a topic of active research interest. The effect of fluid on rock properties has been studied recently in a variety of contexts, including chemical effects,[26] slow dynamics,[21] and mass and length changes.[27] From these and previous works, we divide solid–fluid interactions within rocks during applied stress into two categories. In the first category, fluid migrates or is redistributed internally within the pore structures and/or evaporates from the surface. In the second category, the fluid induces microstructural changes and/or permanent modifications in the solid matrix by water absorption by hydrophilic constituents such as clay (which often exists between grains within the rock) or by deformation of the existing

pore space (via the expansion of existing cracks and pores or the creation of new ones). How rocks interact with moisture is also related to solid–liquid molecular interactions.[16,17,20] Rocks are generally hydrophilic materials and contain a large internal surface area. As a result, absorbed water can significantly influence their non-linear responses by changing internal molecular forces at different levels of saturation. These changes include molecular adsorption forces along pore walls, capillary pressures in pores, and interlayer fluid pressures (due to the presence of interlayer hydrate water in clay particles). Precisely how these different forces influence non-linearity in rocks is still incompletely understood. In addition to improving our understanding of the complex non-linear systems present within rocks, understanding these effects opens up the possibility of using non-linear techniques to characterize fluids *in situ* both in the subsurface and for non-destructive testing.

Experiments that study the interaction between water and rocks are still an active area of research. For example, Ilin *et al.*[27] look carefully at where within the pore space water is held, and Bittner and Popovics[21] look carefully at the fluid within a single pore. However, Ilin *et al.*[27] do not consider non-linear interactions, and Bittner *et al.*[21] report observations of slow dynamics and not fast dynamics, which are easier to initiate. In addition, most of the work on non-linearity and fluids involves systems at resonance.[20,21] However, at the field scale for both nondestructive testing and subsurface characterization, propagating wave experiments are much more practical. In addition, because non-linear responses are often quite sensitive to background conditions like humidity and temperature, it is important to develop experimental methods that do not rely on comparing signals taken at different external conditions.

To study these aspects, we design an experiment that builds on dynamic acoustoelastic testing (DAET). DAET is a noninvasive technique designed to study the mechanisms of non-linear and non-equilibrium dynamics with high sensitivity in small strain regimes (10^{-8}–10^{-5}). This technique is based on two compressional (P-wave) dynamic fields: a low-frequency signal to perturb the material (the pump) and a high-frequency signal to measure the induced changes (the probe). Typically in DAET, the sample is a long thin bar, and the pump excites the sample at the resonant frequency. This mimics the experimental condition in the non-linear resonant ultrasound spectroscopy method (NRUS),[10] where the resonance frequency decreases as a function of strain. In DAET, the probe propagates across the shortest dimension of the bar to reduce the travel time of the probe so that the strain field, induced by the pump, can be assumed to be constant. By comparing the travel time of the probe before excitation and during a number of phases of the pump excitation, the relative changes in the arrival time of the probe are measured and used to assess the non-linearity in the sample.[28–31]

To study the non-linear elastic properties of rocks, we employ DAET with the following four modifications:[14,32–34]

1. Use a large probe source-receiver distance (15.3 cm), compared to the pump wavelength (1.4 cm), to study larger samples,
2. Replace the resonant pump with a propagating pump, to create a non-uniform and non-static strain field which is a first and necessary step to enable the study of larger samples,
3. Use an S-wave or a shear wave pump, instead of a P-wave or a compressional pump, to align the strain field with the direction of propagation of the probe, and
4. Measure the travel time delay relative to a background signal taken immediately before the perturbed signal, rather than at the beginning of the experiment, to minimize the influence of variations in experimental conditions on our data and to allow flexibility for eventually applying the technique at a larger scale.

This modified-DAET method was first introduced by Gallot *et al.*[32] and has been used to study the effect of cracks and their orientations[33,35] and the effect of an applied uni-axial load.[14] This paper aims to characterize the effect of environmental humidity changes on the non-linear response of the rock. We show that our method is able to detect small changes in the non-linear response that are correlated with the amount of time that the sample has been exposed to a change in its environmental humidity. We then use our measurements to characterize the time required to dry or hydrate our sample, recovering a relaxation time to describe this process.

II. METHODS

A. Experimental setup

In our experiments, we monitor the changes in the travel time of a small amplitude probe wave during the propagation of a larger amplitude pump wave. Our experimental setup is shown in Fig. 1(a). We use a rectangular slab, 15.3 × 12.5 × 5 cm^3, of Crab Orchard sandstone that is composed of over 85% quartz and <15% moisture-sensitive clay minerals.[36] During experiments, we orient the block so that the normal to the bedding layers is parallel to the probe and pump particle oscillations; this produces a larger magnitude for the travel time delay.[33,35]

We use an arbitrary waveform generator (Keysight 33500B Series) to create the probe and the pump signals. We generate a one-cycle 700 kHz probe signal with a P-wave transducer with a

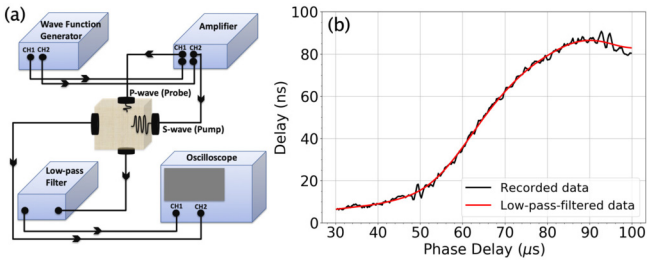

FIG. 1. (a) Experimental setup: a view from the top of the sample: The S-wave pump (right transducer) and P-wave probe (top transducer) produce signals that propagate into the sample. The perturbed probe signal is recorded on the receiver (bottom transducer), and the delay in the probe travel time is measured as a function of phase delay (explained in Fig. 2). Normal to the bedding layers is parallel to the P-wave particle motion (the direction of the propagation). (b) An example of time delay vs phase delay measurement. The raw data and the low-pass-filtered data (f_{cutoff} = 50 kHz) are shown with black and red lines, respectively.

diameter of 1.27 cm (Olympus Panametrics™ V103). For the pump, we use a high-amplitude four-cycle 90 kHz S-wave transmitted from an S-wave transducer with a 2.54 cm diameter (Olympus Videoscan V1548). We choose these frequencies so that the probe wave has a significantly lower wavelength than the pump ($\lambda_{probe} \approx 0.4\,\text{cm} < \lambda_{pump} \approx 1.4\,\text{cm}$). This means that the pump wave is approximately in steady state during the timescale of the probe propagation. We use a P-wave probe and an S-wave pump to allow us to align the particle motions of the two propagating waves. We choose the timing for a probe such that the probe only senses an incident wave, not the reflected one. Thus, the sample essentially can be considered a semi-infinite medium.

All signals for the non-linear experiments are collected with an identical P-wave transducer on the opposite side of the sample from the probe source transducer. We also monitor the S-wave pump signal with an additional S-wave transducer placed opposite the pump source to allow us to monitor changes in the pump signal during the experiments. Both input signals are amplified (Tegam Model 2350). We use a Butterworth high-pass frequency filter (Krohn-Hite Model 3940), with cut-off frequencies of 400 or 600 kHz, to minimize the amplitude of the pump signal measured at the receiver so that we record primarily the probe signal.

All experiments were carried out in a polystyrene foam box that helps to regulate humidity changes. The humidity is monitored with resistance-based humidity sensors (Arduino Uno) placed inside the box. The relative humidity inside the box is reduced as low as possible using a zeolite (silicate) desiccant for drying experiments; for humidity experiments, it is increased as high as possible using a saturated NaCl solution.[37] For the drying experiments, the desiccant is reactivated every 7 days using a microwave for 3 min and subsequently kept at room temperature for an hour to cool-down before it is returned to the polystyrene box. To make the saturated salt solution and to reach a relative humidity near 75% inside the box, we add 280 g of NaCl to 600 ml of water. Since there is no feasible way to measure the relative humidity inside the rock, we report only the relative humidity inside the box. We correlate our results with the amount of time that the sample has spent inside the box during either drying or hydrating stages.

B. Time delay measurements

Our experimental setup is designed to measure the changes in the travel time of the probe. The magnitude of the travel time is an indication of the strength of the non-linearity. The non-linear effect is rather small, with travel time delays on the order of nanoseconds (compared to the 49 μs travel time across the sample). To extract such a small delay, we use a method introduced in the earlier work,[32] which consists of

1. Send and record a probe signal, S_1,
2. Send and record a pump signal, S_2,
3. Send and record a pump and probe signal simultaneously as S_3,
4. Calculate the perturbed probe $S_4 = S_3 - S_2$,
5. Calculate the cross correlation between the probe signal, S_1, and the perturbed probe, S_4, using

$$(S_4{}^*S_1)(\tau) = \int_0^\infty S_1(t)S_4(t+\tau)dt. \quad (1)$$

6. Fit the five points nearest the maximum of the cross correlation to a parabola, the peak of which is taken as the delay between the probe and the perturbed probe.[38]

Representative examples of these four signals are shown in Fig. 2.

For each experiment, we plot the measured probe delay time vs phase delay, such as the example shown in Fig. 1(b). The phase delay (plotted on the horizontal axis) is the amount of time elapsed after the emission of the pump signal before the probe signal is triggered. As we increase the phase delay of the probe, it interacts with more of the pump signal, thereby increasing the delay. The fact that we see only delays, and not advances of the probe signal, is consistent with other results on similar rocks,[28,29,32] as well as theoretical studies[30,32] that predict softening of rocks under applied

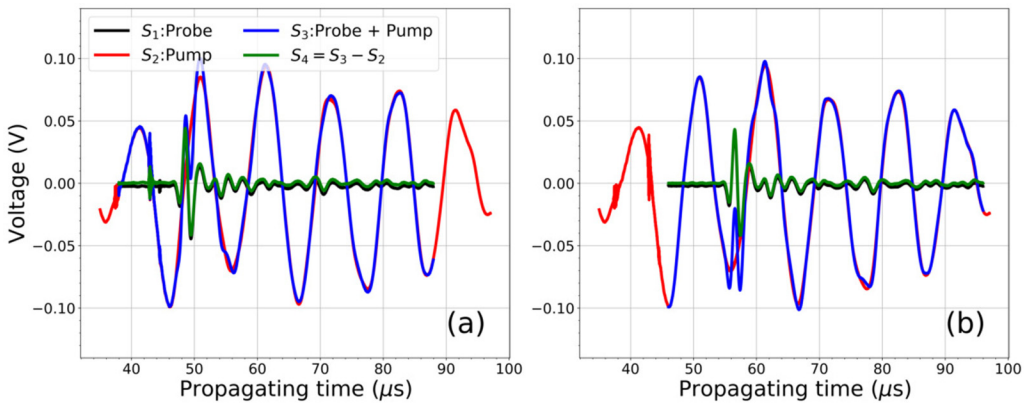

FIG. 2. Voltage vs propagating time where black, red, blue, and green colors represent the S_1: probe, S_2: pump, S_3: probe plus pump, and $S_4 = S_3 - S_2$: subtraction between probe plus pump and the pump signals, respectively. (a) Probe phase delay of 48 μs and (b) probe phase delay of 56 μs, respectively. Each phase delay corresponds to a different phase of the pump signal. We change the phase delay between the probe and the pump signals so that we can use the probe to scan several cycles of the pump.

TABLE I. Table summarizing experimental conditions. The sampling rate refers to the sampling of the phase delay. The relative humidity indicates the variations in the humidity level inside the box: the first value at the beginning of the trial and the second at the end of the trial. The low-pass filter frequency describes the corner frequencies of the high-pass filter used in the experiments.

	Trial 1 (drying)	Trial 2 (hydrating)	Trial 3 (drying)
Pump voltage (V_{0P})	450	450, 100	450, 100
Pump frequency (kHz)	90	90	90
Probe voltage (V_{0P})	100, 250, 400	50, 20, 5	50, 20, 5
Probe frequency (kHz)	700	700	700
Sampling rate (MHz)	1	4	4
Relative humidity (%)	2–(−0)	10–65	15-(−0)
Low-pass filter frequency (kHz)	A value between 400 and 600	A value between 400 and 600	A value between 400 and 600

dynamic stresses. Moreover, if we initiate the pump and the probe at the same time, the probe arrives at the center of the sample before the pump, and the two waves do not interact. However, if we delay the probe, then the probe can be influenced by the pump as they will interact in the middle of the sample. This extra delay is added to the phase delay value while doing the experiment.

Although the delay signals often contain coherent information at multiple frequencies, here we focus on the lowest-frequency component of these signals because it is in this low-frequency part of the signal that we observe the largest response to humidity-induced changes. The higher-frequency part and its attribution to the non-linearity will be studied separately from this paper. To remove the smaller-scale oscillations (high-frequency components), we filter the data with a Butterworth low-pass filter, with a cutoff frequency, a number between 40 and 60 kHz depending on the experiment; this signal is overlaid on the unfiltered data, shown as the red signal in Fig. 1(b).

In all experiments described here, the maximum delay occurs for a phase delay of approximately 90 μs. This time is governed by the geometry of the setup; in other words, if we were to change the mounting positions of the pump and probe transducers, the phase delay at which the maximum delay occurs would also change.

In this work, we consider probe delay times rather than velocities because there is no consistent convention in the existing literature. For convenience, we note that one can easily convert a delay time to a velocity change, using the equation $dV = \frac{-ldT}{T^2}\,(\frac{m}{s})$, where $l = 15.3 \times 10^{-2}$ m is the distance between transducers, dT is the time delay, and T is the arrival time of P-wave.

This paper describes results from two drying trials and one humidification trial. The specifications of each trial are summarized in Table I. In trial 1, the sample had been at room conditions for several months before we began the trial. In trial 3, however, the sample was first humidified during trial 2 and then dried. For trials 1 and 3, the relative humidity decreases to −2% and −1%, respectively (both numbers are reported as −0 in Table I). We think that for trial 3 the box itself was at a higher humidity state due to hydration in trial 2 and since the humidity sensor cannot measure the humidity inside the rock (it only measures the humidity inside the box) the initial humidity value of trial 3 is larger than trial 1. For all trials, the rock is first kept in the humidity-controlled box for 24 h before we carry out the experiments. Each trial lasted more than 2 months, and each measurement (experiment) within a trial takes approximately 2–4 h. It is worth noting that while the sampling rate in trial 1 is 1 MHz, it is 4 MHz for trials 2 and 3.

C. Velocity, strain, and stiffness measurements

In this section, we describe how we measure the particle velocities, calculate the wave velocities, and calculate the strain induced by the probe and pump waves. We note that the experimental setups to measure these quantities are different than that shown in Fig. 1(a). For these measurements, the sample was maintained at room temperature and humidity, which means that it was not fully desiccated. These results are summarized in Table II.

We measure the pump and probe surface particle velocities, $V_{probe}^{Particle}$ and $V_{pump}^{Particle}$, with a compact laser vibrometer (Polytek CLV-2534). The setup is composed of five components: a transducer, a laser vibrometer, a vibration isolation table, a function generator to produce the input signal, and an oscilloscope to record the output signal. We use the transducer as the source (connected to the function generator) and the laser vibrometer as the receiver. The sample and the laser (on a translation stage) were both mounted on an optical breadboard, with no active vibration isolation. The translation stage and optical breadboard allow us reliable relative positioning between the sample and the laser. The laser vibrometer records the amplitude of particle vibrations vs time, and this signal is seen and recorded by an oscilloscope connected to the laser vibrometer. We consider the maximum amplitude of each signal as the particle velocity in the following calculations.

TABLE II. Experimental parameters for strain measurements. The first three parameters are physical properties of the Crab Orchard Sandstone sample. The last four ($V_{probe}^{Particle}$ to ε_{pump}) are measured during the strain-evaluation experiment.

ρ (kg m^{-3})	2300
V_{probe} (m s^{-1})	3130
V_{pump} (m s^{-1})	1280
t_{probe} (s)	48.8×10^{-6}
t_{pump} (s)	119×10^{-6}
$V_{probe}^{Particle}$ (m s^{-1})	12.9×10^{-5}
$V_{pump}^{Particle}$ (m s^{-1})	41.6×10^{-3}
ε_{probe}	4.1×10^{-8}
ε_{pump}	1.6×10^{-5}

We measure the $V^{Particle}_{probe/pump}$ at several different locations on the sample, including the middle and the edge of the sample. The average of all measurements is reported in Table II.

To measure the velocity of the two waves, V_{probe} and V_{pump}, we use a setup with four components: two identical transducers, a function generator, and an oscilloscope. The two transducers are attached to the opposite sides of the sample, where one is the source (connected to the function generator) and the other one is the receiver (connected to the oscilloscope). The receiver records the output signal from which we estimate the arrival time. The velocity of the two waves, V_{probe} and V_{pump}, is calculated using

$$V_{probe/pump} = \frac{d}{t_{probe/pump}}, \tag{2}$$

where $d = 15.3$ cm is the distance between the source and the receiver and t_{probe} and t_{pump} are the arrival time of individual waves.

We next calculate the strain. Strain can be roughly estimated using

$$\varepsilon_{probe/pump} \approx \alpha \left| \frac{V^{Particle}_{probe/pump}}{V_{probe/pump}} \right|, \tag{3}$$

where $\alpha = 1$ for probe and $\alpha = 1/2$ for pump. This expression is exact for plane wave propagation and is derived in the supplementary material. As indicated in Table II, the strain induced by the pump is three orders of magnitude larger than that for the probe. Because of the large difference in the applied strains, we assume that perturbations to the sample are caused by the pump and sensed by the probe.

It is important to note that $V^{Particle}_{probe/pump}$—and hence the strain—depends strongly on the probe and pump voltages. In contrast, $t_{probe/pump}$ depends on the sample size and geometry, while $V_{probe/pump}$ is a physical property of the rock. For different values of these two voltages, one needs to scale the strains summarized in Table II. The reported values of the strain in that table are for a pump voltage of 450 V and a probe voltage of 10 V. The frequencies of both pump and probe are those listed in Table I.

III. RESULTS

A. Effect of humidity on the non-linear response

Figure 3 compares the low-pass-filtered arrival time delays of the probe as a function of the phase delay. When the sample is continuously dried [Fig. 3(a)], the amplitude of the delay decreases; when the sample is continuously humidified [Fig. 3(b)], the delay amplitude increases. These trends hold for all pump and probe amplitudes that we investigated (as listed in Table I). Over the course of one complete drying or hydrating trial, the net sample weight change is 2–3 g, which is approximately 0.1% of the total sample weight. It is well established that the velocity decreases (increases) with increasing (decreasing) humidity and the attenuation increases (decreases) with increasing (decreasing) humidity.[39]

Further analysis of the time delay measurements shows that the time delay changes follow an exponential relation as a function of the length of time the sample has spent in the humid

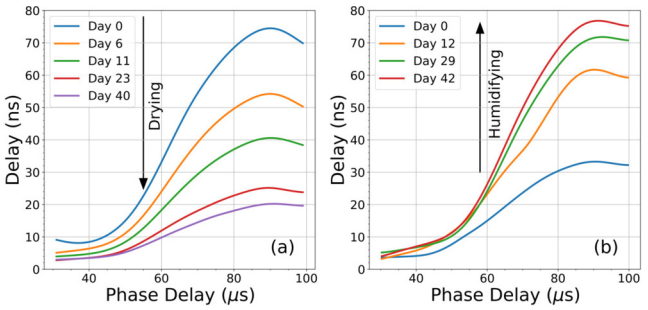

FIG. 3. Effect of humidity on the non-linear signal: (a) and (b) show how the amplitude of the low-pass-filtered delay [$f_{cutoff} = 40$ for (a) and 60 kHz for (b)] decrease and increase as the rock dries and humidifies, respectively. The legends indicate the number of days since the rock was placed in the dry or humid environment.

environment. An example of exponential decay for different values of phase delay is shown in Fig. 4. We see that the data (circles) are well fit by exponential functions,

$$Y = a + b \times \exp(-(x - c)/\tau), \tag{4}$$

that are overlaid as solid lines. Figure 5 shows the exponential relation for different combinations of probe and pump amplitudes at a phase delay of 92 μs. We note that the initial values of the delay (at time = 0), in Fig. 5(a), are not consistent from trial to trial, due to different initial humidification levels inside the rock, since we did nothing special to try to make them identical. It is well established that rocks have a memory of their past conditions, and so we

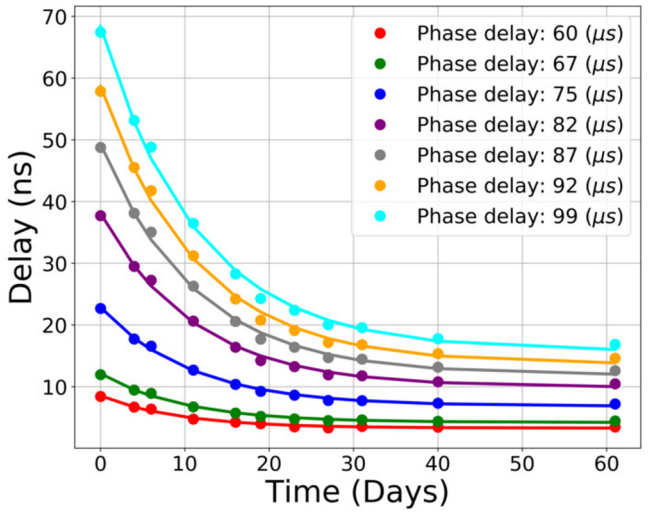

FIG. 4. Data (circles) and corresponding exponential fits (lines) for time delay vs time, measured over a range of different phase delays (60–100 μs). An example of trial 1, which is a drying trial, with probe amplitude = 100 V.

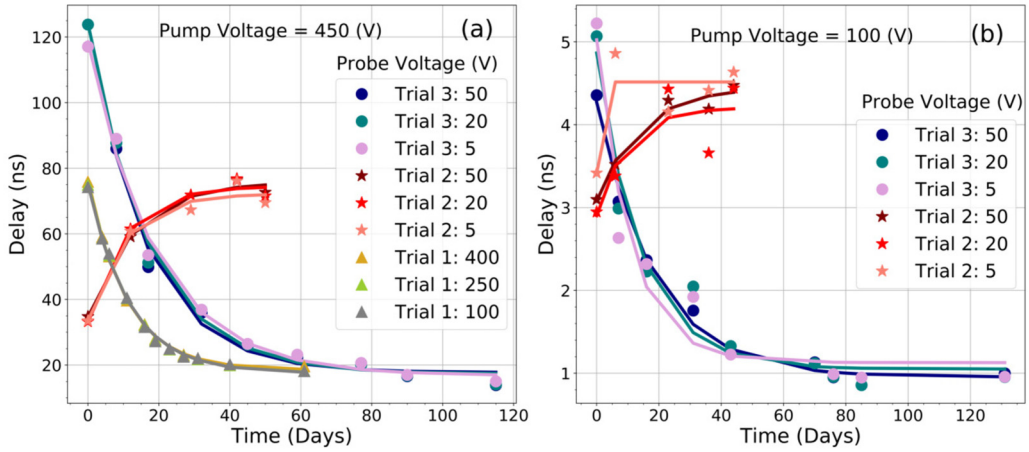

FIG. 5. Time delays plotted as a function of the time the rock has spent in its dry or humid environment at two different pump amplitudes [(a) = 450 V and (b) 100 V]. Drying or hydrating causes changes in the time delay that are well fit by exponential fits (solid lines). The legends show the probe amplitude for different measurements; the phase delay was fixed at 92 μs.

expect this memory plays a role in the initial maximum delay. As each trial adds to the rock's history, it is expected that this maximum value is not repeatable. However, other trends are very solid. For a given trial, the amplitude of the probe does not affect the amplitude of the delay time. However, lowering the pump amplitude does decrease the amplitude of the delay: for example, comparing the data for a stronger pump in Fig. 5(a) with the data for a weaker pump in Fig. 5(b).

The exponential behavior itself is very robust: the characteristic time constants, τ, extracted for all experiments using Eq. (4) are summarized in Fig. 6, with an average value of $\tau \simeq 13$ days. The weighted average is calculated by weighting the measurements using their standard deviation, $M_W = \sum(n/\sigma_n)/\sum(1/\sigma_n) = 13$, where n is the measurement and σ_n is the standard deviation of that measurement. The time constant is independent of the phase delay at which we study the trend (ranging between 60 and 100 μs), and it is also independent of probe amplitude, pump amplitude, and sampling rate. Based on similar values of τ for different experimental conditions, we conclude that our testing conditions show reversible drying/hydrating time constants and if there are any permanent changes (or effects at a significantly longer timescale than our experiments) to the sample due to cycling the humidity conditions, it does not change the time constant.

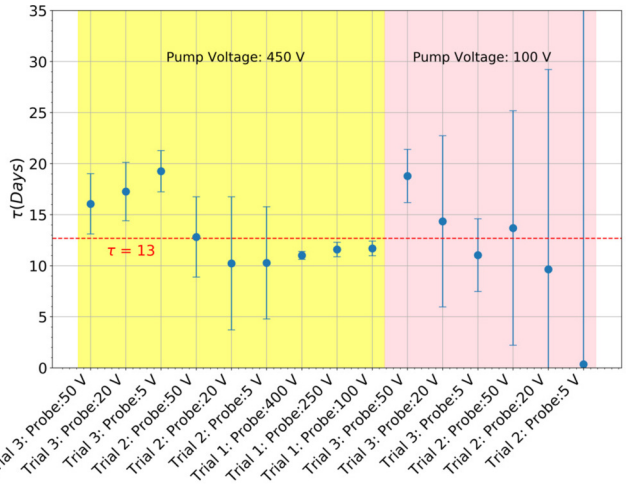

FIG. 6. The time constant, τ, calculated for all trials using Eq. (4) with a weighted average of 13 days.

B. Evolution of pump and probe signals: A linear effect

In addition to changing the non-linear interactions of the pump and probe waves, hydrating or drying affect the amplitudes of the probe and the pump signals, triggering a decrease or an increase, respectively. Figure 7(a) shows an example of an increase in the probe amplitude with time as the sample dries. We study the change in the amplitudes by tracking the normalized maximum of the envelope of the signals, shown in Fig. 7(b). More specifically, we measure the envelope of the signal (absolute value of the Hilbert transform) and take the maximum of this envelope. Taking the envelope removes any effects on the amplitude from the changing phase of the signal. We then normalize this value by dividing it by the maximum observed in that experimental trial. Another example is shown in Fig. 7(d), where the amplitude of the pump decreases (from 1 to below 0.25 in the course of 10 days). The pump amplitude is a dominant effect in changing the maximum delay, as we see in Fig. 7(e) and also by comparing the maximum of delay in parts (a) and (b) of Fig. 5. The non-linear response decreases (increases) with drying (hydrating), whereas the amplitude of the pump increases (decreases). It is worth mentioning

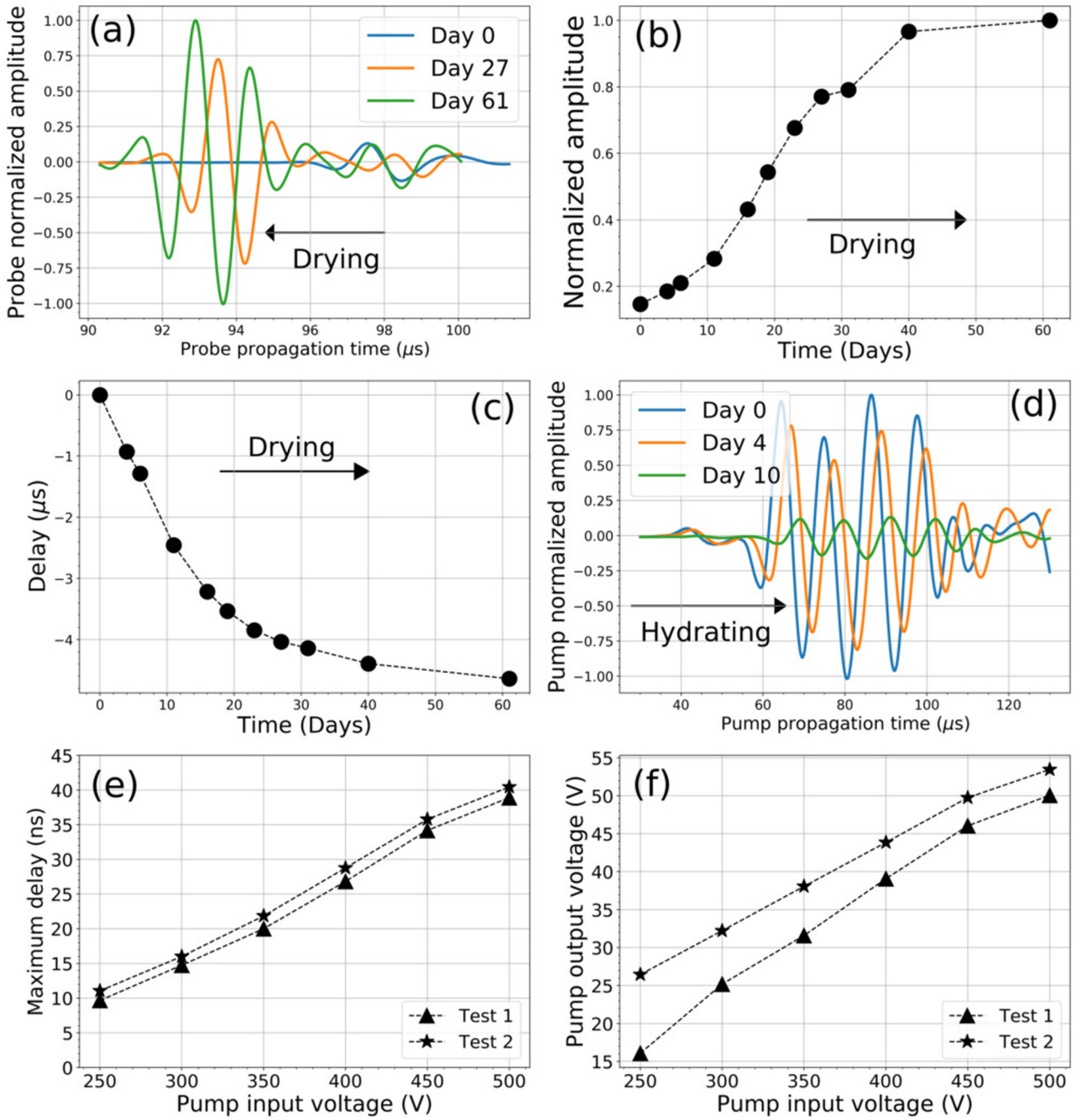

FIG. 7. (a) Representative probe signals show that the amplitude increases and the signal shifts to earlier times as the sample dries (probe = 100 V). (b) The evolution of the probe amplitudes calculated by taking the peak of the envelope of each signal and dividing it by the maximum amplitude observed in that trial. (c) The probe signal shift, measured as the cross correlation peak between the first and subsequent signals. (d) Representative pump signals show an amplitude decrease and a shift to later times as the sample hydrates (pump = 450 V). (e) Test experiments show that there is a linear increase in the maximum probe delay with increasing pump input voltage, while the sample is at a constant humidity level. In other words, the non-linearity is linearly proportional to the pump voltage/amplitude. (f) The same test experiments also show a linear relation between the pump input voltage and the pump output voltage. In (e) and (f), experiments are cycled from the lowest to highest voltage and then back, which means the rock is conditioned differently between tests 1 and 2. In (b), (c), (e), and (f), the lines connecting the data points merely serve as guides to the eye.

that, although the electromagnetic noise/interference is larger when the chamber is humid, the primary reason for larger uncertainties [noisier data in Fig. 5(b) and larger error bars in Fig. 6] at more humidified states is because the amplitude of both pump and probe signals drop as the sample hydrates. Figure 7(f) shows the linear relationship between the input and the output pump amplitudes.

Arrival times of the probe and pump change with humidity. This means that drying speeds the arrival time [Fig. 7(a)] and hydrating delays the signal [Fig. 7(d)]. The change in arrival times is measured as the shift in the peak of cross correlation between the first pulse and consecutive ones, using the same method we used to measure the delays between S_1 and S_4 discussed above. An example of the trend is summarized in Fig. 7(c). Travel time measurements indicate that varying the humidification level of the sample affects not only the delay measurements (Fig. 3), but it also advances or delays the arrival time of the individual probe and pump signals. The advance is shown by negative measured delays in Fig. 7(c). Negative delay times are not problematic because we always compare signals recorded one after another; this means that both S_1 and S_4 will be delayed or advanced by the same amount, and thus it is only the perturbation caused by the pump that changes in the short time of the experiment.

To summarize, the probe and the pump are influenced by the sample hydration level in similar ways at several levels, known as linear effects. First, both the signals are delayed (sped up) as the sample hydrates (dries). Second, signal amplitudes increase as the sample dries and decrease as it hydrates. It is established that the consistency of transducer/sample coupling can be an issue for non-linear experiments. Although it is possible that humidity changes also change the coupling of our transducers to our samples, we expect that this is a minor effect because the waveforms remain similar for much of the process and when they do change (see Fig. 7) the signal amplitudes are reduced (which could indicate poorer coupling) in the humid case when we actually see a larger nonlinear response.

It should be noted that the non-linear measurement is a much more sensitive tool to identify the weakening/softening. We can demonstrate this by comparing the changes in the non-linear delay response [Fig. 3(a), from 20 to about 80 ns] to the changes in the linear delay response [from 0 to about 5 μs in Fig. 7(c)]. Unfortunately, the non-linear tool is also more sensitive to experimental conditions such as the transducer coupling with the sample. This means that, overall, it is easier to measure the linear arrival delay response in a repeatable way, but the non-linear response is more sensitive.

IV. DISCUSSION

To summarize our experimental approach, we change the relative humidity of the rock's environment and then measure the delay in the arrival time of a P-wave (probe), induced by its interactions with an S-wave (pump). The magnitude of the delay is an indication of the strength of the non-linearity induced by the pump.

Our main experimental result is that the amount the pump pulses soften the rock (measured as a travel time delay in the probe wave) is larger in humidified rocks than it is in dried rocks. We find that this process is repeatable and reversible. In addition, the time constant associated with this process (summarized in Fig. 6) is independent of the amplitudes of the pump and the probe, the phase delay, the sampling rate, and whether the sample is being dried or humidified. There are two aspects of this result that merit further discussion. First, these humidity-dependent differences in the amount of softening are induced by only a very small amount of absorbed water vapor. Second, our pump–probe experiments detect these humidity-dependent differences in the amount of softening easily and repeatably using an experimental design that does not rely on resonance conditions. This means that, in principle, our experiments could be more easily generalized to other experimental geometries.

A. Effects of water vapor on the non-linear response in sandstone

During the humidification process, our sample gains mass $\leq$ 3 g (in a 2.86 kg rock) by absorbing water. A straightforward calculation (provided in the supplementary material) shows that this amount of water would correspond to either a thin layer of water ($\approx 2.5 \times 10^{-5}$ cm $= 0.25$ μm thick) over the entire pore space or fill only a small percentage of the pores completely (5%). Although this seems like too little water to have a significant effect, there are other studies at similar saturation levels that provide helpful context for our work. For instance, an early study on the Lavoux limestone shows a dramatic jump in the so-called hysteretic non-linear response for saturation levels less than 0.1%.[20]

A recent study by Ilin *et al.*[27] on another sandstone (Berea sandstone) provides another useful comparison point. It describes a fully water-saturated sandstone that dries gradually in a desiccated environment. During the process of drying, they monitor the mass and length changes to show that most of the water is contained in the larger pores (the void space between the grains of the sandstone) and most of the water leaves the rock relatively quickly (in approximately 1 h). But a small amount of residual water, trapped between clay particles that glue the sand grains together, leaves the sample much more slowly (in days). They also report changes in sample length during the saturation and dehydration experiments, stating that the sample extends while hydrating and shrinks after fully drying. To explain these observations, they draw on a wealth of earlier literature that shows that water intercalation —even in small amounts—will expand clay, and from this they reason that this is sufficient to explain the presence of residual water and length changes. They attribute the shrink in the drying state to the permanent changes in the internal structures and composition of the clay particles.

Some aspects of our experimental results are compatible with the explanations that Ilin *et al.* propose in their experiments once only residual water is present. First, we have a fractional mass change due to water absorption near 2.5 g/2860 g $\approx$ 0.09%, which is on the same order of magnitude as their residual (fractional) water amount 0.001 g/1.8 g $\approx$ 0.06%. Second, the characteristic relaxation time (τ) in our experiments is on the order of days. Given that we used very different sample shapes (ours was a rectangular slab while theirs was cylindrical) and the volume of our sandstone was ~1600 times larger than theirs, our long characteristic

relaxation times (τ) are qualitatively consistent with the time span they required to see their residual water evaporate from the sample. Third, we observe that longer arrival times do indeed occur for our most humidified conditions. This is consistent with the scenario in which more humidification leads to more swelling in the clay portion of the rock, which causes expansion, and which would also cause a longer travel time across the rock.

We see similar timescales for the drying and hydrating processes, suggesting that this process is reversible in our rock. Ilin *et al.* conclude that their drying process is not reversible because they see permanent length changes after saturating and then drying their rock, which they attribute to rearrangement of the clay particles after saturation. This means that the reversible drying/hydrating behavior in our samples could come from a different distribution of water within the pores and clays in our sample that does not trigger changes in the clay structure. Taking all of these pieces of evidence together leads us to believe that we are introducing (removing) water vapor into (from) the clay particles when we are hydrating (drying) our samples.

To further explore the relative importance of water that is intercalated into clay particles and how water in the pore space changes the non-linear response, we look at it from a theoretical perspective. Kim and Guyer[17] explicitly discuss the theory behind the coupling between solids and liquids in porous media. They explain that materials with small pores have large pore-surface/fluid-surface forces, whereas in materials with larger pores a fraction of the fluid molecules are adsorbed on the solid surfaces of the pores. As the relative humidity of the air in the pore-space increases, so does the thickness of the adsorbed water layer. This leads to capillary condensation and eventually to the formation of menisci between the liquid water and the gas phase. The capillary pressure decreases with increasing saturation level, resulting in both softening and expanding the material. The effect of capillary pressure on the solid matrix is also mentioned in Ref. 20. Kim and Guyer[17] also argue that when the sizes of the pores are on the order of the range of molecular interactions, this gives rise to a mechanical pressure orthogonal to the interface, again leading to softening and lengthening. At higher humidity levels, these forces also modify the nanostructure of the material by widening existing gaps. We would expect that our sample, like most sandstones, contains pores from roughly the size of the grains (a fraction of a mm) to the nm scale. Thus, through a combination of these two mechanisms, saturation leads to a softer solid matrix with smaller elastic moduli and a larger non-linear response. This is exactly what we observe here and is consistent with the idea that we are primarily saturating the smaller-scale pores. We also note that the theory of Kim and Guyer is consistent with the expansion observed in Ref. 27.

Our results indicating that the non-linear response is controlled by water in the smaller-scale voids between the clay particles, at first seem to be in contrast to the results in Ref. 21. In that work, Bittner *et al.* present SEM images of the rock's surface before and after acoustic excitation. Their images indicate that strong resonant excitations move water in and out of larger-scale pores (tens to hundreds of micrometers). They then correlate that movement to changes in the non-linear response of the system. The key difference between the experiments of Bittner *et al.* and those presented here is that they link the water movement in these large pores to slow dynamics at the surface.[9] In contrast, we are measuring changes in the fast dynamics due to the changes in the humidity in the bulk of the sample.

Absorption of a small amount of water in different rocks, such as limestone and sandstone[39] and lunar rocks,[40] has been found to have a dramatic effect on the attenuation. Two mechanisms of attenuation are presented: first at very small amounts of water absorption, two mono-layers of water, which is associated with surface interaction of the water molecules and grain, and second at higher values, which is related to condensation of sufficient amount of water in the pores to obtain fluid flow. It was also shown that most of the increase in attenuation happens with the absorption of the first two mono-layers of water. Clark *et al.*[39] say that a small amount of water (with the corresponding surface coverages of two mono-layers) that does not affect the density of sandstone should not affect the seismic velocity. In our experiments, we have very little density change, but our rock also has relatively low porosity, which we estimate would result in pore coverages that would be on the order of 1000 water layers thick in the pore space. This could explain why we see a significant change in the arrival time of probe while exposing the rock to a humid environment.

Finally, we note that our relaxation time, $\tau \approx 13$ days, would very likely depend on the microstructures of the sample and thus that it would vary from sample to sample. This means that we do not ascribe any specific significance to the exact value of τ.

B. Advantages of using propagating rather than resonant waves

We are not the first to have noticed that small amounts of water can have an effect on the non-linear responses of sandstone.[20] However, our pump–probe experiments detect softening easily and repeatably using an experiment design that does not rely on resonance conditions, which makes our experiments different than many previous studies. In a resonance experiment, one can exploit the geometric shape of the sample to detect changes in resonant frequencies as a function of drive amplitude. For example, in resonance experiments, Lavoux limestone shows a dramatic jump in the so-called hysteretic non-linear response for saturation levels less than 0.1%.[20] In contrast, our experiments use a finite pump pulse as well as a finite probe pulse. Although the interaction area of these waves is potentially difficult to specify, our assessments of softening are repeatable and independent of the amplitudes of the pump and the probe, the phase delay, and the sampling rate. As an example, Fig. 6 shows the consistency across different pump and probe amplitudes of our time constant that corresponds to drying/hydrating. Furthermore, because our experiments are always comparing a perturbed and unperturbed probe wave, we are less sensitive to changes in environmental conditions during our experiments. (It is difficult to imagine significant changes between sending the pump alone and pump/probe together a few ms later.) This comparative method of studying the non-linearity is also useful in noisy environments when we are trying to extract small non-linear signals from the background noise because taking the difference reduces the influence of the noise. Therefore, in principle, our method could be more easily generalizable to other experimental geometries and

other materials. Some preliminary work has been done to address localized changes in the rock.[41] This, however, remains an open problem for this experimental configuration.

V. CONCLUSION

The propagating mode adaptation of the DAET technique that we use is a powerful way to study the effect of ambient humidity on the non-linear interactions of two propagating acoustic waves. We show that there is a time constant ($\tau \approx 13$ days) that is consistent over a range of different pump and probe amplitudes, with different phase delays between the pump and the probe, and changes in the sampling rate. This means that the humidity-dependent differences in the amount of softening are very robust and not influenced by our choice of measurement conditions. Evidence from our and other work suggests that it is the water within the smallest pores that control the observed behavior.

SUPPLEMENTARY MATERIAL

See the supplementary material for a derivation of Eq. (3) and a rough estimation of the thickness of water layer in pore space.

ACKNOWLEDGMENTS

Funding from the Natural Sciences and Engineering Research Council of Canada (NSERC, Grant Nos. IRCPJ 491051-14 and 2018-04888) as well as from Chevron and InnovateNL (Grant No. 5404-1085-104) is acknowledged.

REFERENCES

[1]R. A. Guyer and P. A. Johnson, "Nonlinear mesoscopic elasticity: Evidence for a new class of materials," Phys. Today **52**, 30 (1999).
[2]L. A. Ostrovsky and P. A. Johnson, "Dynamic nonlinear elasticity in geomaterials," Riv. Nuovo Cimento Soc. Ital. Fis. **24**, 1–46 (2001).
[3]R. A. Guyer and P. A. Johnson, *Nonlinear mesoscopic elasticity: The complex behaviour of rocks, soil, concrete*, 1st ed. (Wiley-VCH, 2009).
[4]N. G. W. Cook and K. Hodgson, "Some detailed stress-strain curves for rock," J. Geophys. Res. **70**, 2883–2888, https://doi.org/10.1029/JZ070i012p02883 (1965).
[5]R. A. Guyer, K. R. McCall, and G. N. Boitnott, "Hysteresis, discrete memory, and nonlinear wave propagation in rock: A new paradigm," Phys. Rev. Lett. **74**, 3491–3494 (1995).
[6]J. A. TenCate and T. J. Shankland, "Slow dynamics in the nonlinear elastic response of Berea sandstone," Geophys. Res. Lett. **23**, 3019–3022, https://doi.org/10.1029/96GL02884 (1996).
[7]R. A. Guyer, K. R. McCall, and K. Van Den Abeele, "Slow elastic dynamics in a resonant bar of rock," Geophys. Res. Lett. **25**, 1585–1588, https://doi.org/10.1029/98GL51231 (1998).
[8]J. A. TenCate, E. Smith, and R. A. Guyer, "Universal slow dynamics in granular solids," Phys. Rev. Lett. **85**, 1020–1023 (2000).
[9]J. A. TenCate, "Slow dynamics of earth materials: An experimental overview," Pure Appl. Geophys. **168**, 2211–2219 (2011).
[10]P. A. Johnson, B. Zinszner, and P. N. J. Rasolofosaon, "Resonance and elastic nonlinear phenomena in rock," J. Geophys. Res. Solid Earth **101**, 11553–11564, https://doi.org/10.1029/96JB00647 (1996).
[11]R. A. Guyer, J. TenCate, and P. Johnson, "Hysteresis and the dynamic elasticity of consolidated granular materials," Phys. Rev. Lett. **82**, 3280–3283 (1999).
[12]K. R. Mccall and R. A. Guyer, "A new theoretical paradigm to describe hysteresis, discrete memory and nonlinear elastic wave propagation in rock," Nonlinear Process. Geophys. **3**, 89–101 (1996).
[13]R. A. Guyer, K. R. McCall, G. N. Boitnott, L. B. Hilbert, and T. J. Plona, "Quantitative implementation of Preisach-Mayergoyz space to find static and dynamic elastic moduli in rock," J. Geophys. Res. Solid Earth **102**, 5281–5293, https://doi.org/10.1029/96JB03740 (1997).
[14]L. O. Hayes, A. Malcolm, K. Moravej, and S. D. Butt, "Nonlinear interactions of P and S waves under uniaxial stress," Proc. Meetings Acoust. **34**, 045012 (2018).
[15]C. Sens-Schönfelder, R. Snieder, and X. Li, "A model for nonlinear elasticity in rocks based on friction of internal interfaces and contact aging," Geophys. J. Int. **216**, 319–331 (2019).
[16]J. Carmeliet and K. E. A. Van Den Abeele, "Mesoscopic approach for modelling the nonlinear hysteretic response of damaged porous media in quasi-static and dynamic loading: effects of pressure and moisture saturation," in *Proceedings of the 4th International Conference on Fracture Mechanics of Concrete and Concrete Structures* (2001), pp. 11–18.
[17]*Nonlinear elasticity and hysteresis: Fluid-solid coupling in porous media*, edited by A. H. Kim and R. A. Guyer (Wiley-VCH, 2015), Chap. 4, pp. 94–96.
[18]O. O. Vakhnenko, V. O. Vakhnenko, and T. J. Shankland, "Soft-ratchet modeling of end-point memory in the nonlinear resonant response of sedimentary rocks," Phys. Rev. B **71**, 174103 (2005).
[19]L. Bocquet, E. Charlaix, S. Ciliberto, and J. Crassous, "Moisture-induced ageing in granular media and the kinetics of capillary condensation," Nature **396**, 735–737 (1998).
[20]K. E. A. Van Den Abeele, J. Carmeliet, P. A. Johnson, and B. Zinszner, "Influence of water saturation on the nonlinear elastic mesoscopic response in Earth materials and the implications to the mechanism of nonlinearity," J. Geophys. Res. Solid Earth **107**, 1–11, https://doi.org/10.1029/2001JB000368 (2002).
[21]J. A. Bittner and J. S. Popovics, "Direct imaging of moisture effects during slow dynamic nonlinearity," Appl. Phys. Lett. **114**, 021901 (2019).
[22]L. Pimienta, J. Fortin, and Y. Guéguen, "Investigation of elastic weakening in limestone and sandstone samples from moisture adsorption," Geophys. J. Int. **199**, 335–347 (2014).
[23]A. Yurikov, M. Lebedev, G. Y. Gor, and B. Gurevich, "Sorption-induced deformation and elastic weakening of Bentheim sandstone," J. Geophys. Res. Solid Earth **123**, 8589–8601, https://doi.org/10.1029/2018JB016003 (2018).
[24]L. Pimienta, C. David, J. Sarout, X. Perrot, J. Dautriat, and C. Barnes, "Evolution in seismic properties during low and intermediate water saturation: Competing mechanisms during water imbibition?," Geophys. Res. Lett. **46**, 4581–4590, https://doi.org/10.1029/2019GL082419 (2019).
[25]M. Tiennot and J. Fortin, "Moisture-induced elastic weakening and wave propagation in a clay-bearing sandstone," Geotech. Lett. **10**, 424–428 (2020).
[26]T. Vanorio, "Recent advances in time-lapse, laboratory rock physics for the characterization and monitoring of fluid-rock interactions," Geophysics **80**, WA49–WA59 (2015).
[27]E. Ilin, M. Marchevsky, I. Burkova, M. Pak, and A. Bezryadin, "Nanometer-scale deformations of Berea sandstone under moisture-content variations," Phys. Rev. Appl. **13**, 024043 (2020).
[28]G. Renaud, S. Callé, and M. Defontaine, "Remote dynamic acoustoelastic testing: Elastic and dissipative acoustic nonlinearities measured under hydrostatic tension and compression," Appl. Phys. Lett. **94**, 011905 (2009).
[29]J. Rivière, G. Renaud, R. A. Guyer, and P. A. Johnson, "Pump and probe waves in dynamic acousto-elasticity: Comprehensive description and comparison with nonlinear elastic theories," J. Appl. Phys. **114**, 011905 (2013).
[30]M. Lott, C. Payan, V. Garnier, Q. A. Vu, J. N. Eiras, M. C. Remillieux, P.-Y. Le Bas, and T. J. Ulrich, "Three-dimensional treatment of nonequilibrium dynamics and higher order elasticity," Appl. Phys. Lett. **108**, 141907 (2016).
[31]M. C. Remillieux, T. J. Ulrich, H. E. Goodman, and J. A. Ten Cate, "Propagation of a finite-amplitude elastic pulse in a bar of Berea sandstone: A detailed look at the mechanisms of classical nonlinearity, hysteresis, and non-equilibrium dynamics," J. Geophys. Res. Solid Earth **122**, 8892–8909, https://doi.org/10.1002/2017JB014258 (2017).
[32]T. Gallot, A. E. Malcolm, T. L. Szabo, S. Brown, D. Burns, and M. Fehler, "Characterizing the nonlinear interaction of S- and P-waves in a rock sample," J. Appl. Phys. **117**, 034902 (2015).

[33]J. A. TenCate, A. E. Malcolm, X. Feng, and M. C. Fehler, "The effect of crack orientation on the nonlinear interaction of a P wave with an S wave," Geophys. Res. Lett. **43**, 6146–6152, https://doi.org/10.1002/2016GL069219 (2016).
[34]L. O. Hayes and A. Malcolm, *How fracture orientation and particle motion impact nonlinear interactions in an elastic medium* (Society of Exploration Geophysicists, 2017), pp. 3961–3965.
[35]H. Rusmanugroho, A. Malcolm, and M. Darijani, "A numerical model for the nonlinear interaction of elastic waves with cracks," Wave Motion **92**, 102444 (2020).
[36]P. M. Benson, P. G. Meredith, and E. S. Platzman, "Relating pore fabric geometry to acoustic and permeability anisotropy in crab orchard sandstone: A laboratory study using magnetic ferrofluid," Geophys. Res. Lett. **30**(19), SDE 1–4 (2003).
[37]L. B. Rockland, "Saturated salt solutions for static control of relative humidity between 5 and 40 °C," Anal. Chem. **32**, 1375–1376 (1960).
[38]S. Catheline, F. Wu, and M. Fink, "A solution to diffraction biases in sonoelasticity: The acoustic impulse technique," J. Acoust. Soc. Am. **105**, 2941–2950 (1999).
[39]V. A. Clark, B. R. Tittmann, and T. W. Spencer, "Effect of volatiles on attenuation (Q-1) and velocity in sedimentary rocks," J. Geophys. Res. **85**, 5190–5198, https://doi.org/10.1029/JB085iB10p05190 (1980).
[40]B. R. Tittmann, V. A. Clark, J. M. Richardson, and T. W. Spencer, "Possible mechanism for seismic attenuation in rocks containing small amounts of volatiles," J. Geophys. Res. **85**, 5199–5208, https://doi.org/10.1029/JB085iB10p05199 (1980).
[41]T. Gallot, A. E. Malcolm, D. Burns, S. Brown, M. Fehler, and T. L. Szabo, *Nonlinear interaction of seismic waves in the lab: A potential tool for characterizing pore structure and fluids* (Society of Exploration Geophysicists, 2014), pp. 2743–2748.

A non-linear elastic approach to study the effect of ambient humidity on sandstone

Somayeh Khajehpour Tadavani,[1, a)] Kristin M. Poduska,[1] Alison E. Malcolm,[2, b)] and Andrey Melnikov[2]
[1)] *Department of Physics and Physical Oceanography, Memorial University, St. John's, Newfoundland and Labrador, Canada, A1B 3X7*
[2)] *Department of Earth Sciences, Memorial University of Newfoundland, St. John's, Newfoundland and Labrador, Canada, A1B 3X5*

(Dated: 3 December 2020)

I. SUPPLEMENTARY MATERIAL

The supporting Material includes two parts: a derivation of Equation 3 of the manuscript and a rough estimation of thickness of water layer in the pore space.

A. Strain calculations

In general, the displacement of a plane wave is

$$\mathbf{u}(\mathbf{x},t) = \mathbf{m} f(\mathbf{n}\cdot\mathbf{x} - ct), \tag{1}$$

where f is a function that is at least once differentiable, the unit vector $\mathbf{m}$ represents the direction of displacement (polarization), the unit vector $\mathbf{n}$ is the direction of propagation of the wave, c is the wave speed, and t is the time. For example, see in[1].

Let us consider a wave propagating in the direction x_1 with the same direction in the polarization x_1 (longitudinal wave). Thus, we can write

$$u_1(x_1,t) = m_1 f(x_1 - ct). \tag{2}$$

The velocity of an oscillating particle will be

$$v_1(x_1,t) = \frac{\partial u_1(x_1,t)}{\partial t} = m_1 f'(x_1 - ct)\cdot(-c). \tag{3}$$

In general, for three dimensions the components of a strain tensor are

$$\varepsilon_{ij} = \frac{1}{2}\left(\frac{\partial u_i}{\partial x_j} + \frac{\partial u_j}{\partial x_i}\right), \tag{4}$$

where $i, j \in \{1,2,3\}$.

Using equation (4), for a longitudinal wave, we have

$$\varepsilon_{11} = \frac{\partial u_1(x_1,t)}{\partial x_1} = m_1 f'(x_1 - ct) = -\frac{v_1(x_1,t)}{c},$$

where we have also used (3).

Now, let us consider a transverse wave propagating in the x_1-direction with polarization in the x_2-direction. In this case

$$u_2(x_1,t) = m_2 f(x_1 - ct).$$

As for the longitudinal wave, the velocity of an oscillating particle is

$$v_2(x_1,t) = \frac{\partial u_2(x_1,t)}{\partial t} = m_2 f'(x_1 - ct)\cdot(-c). \tag{5}$$

The only non-zero components of the strain tensor from expression (4) are

$$\begin{aligned}\varepsilon_{21} = \varepsilon_{12} &= \frac{1}{2}\left(\frac{\partial u_1}{\partial x_2} + \frac{\partial u_2}{\partial x_1}\right)\\ &= \frac{1}{2} m_2 f'(x_1 - ct) = -\frac{1}{2}\frac{v_2(x_1,t)}{c}.\end{aligned} \tag{6}$$

Similarly, for a transverse wave propagating in the direction x_1 and polarized in the direction x_3, we obtain

$$\begin{aligned}\varepsilon_{31} = \varepsilon_{13} &= \frac{1}{2}\left(\frac{\partial u_3}{\partial x_1} + \frac{\partial u_1}{\partial x_3}\right)\\ &= \frac{1}{2} m_3 f'(x_1 - ct) = -\frac{1}{2}\frac{v_3(x_1,t)}{c},\end{aligned} \tag{7}$$

as the only non-zero components of the strain tensor.

B. Thickness of water layer

If we assume that our sample has a porosity of 5%, which is the value measured on rock from the same quarry by[?] , then we can expect to have at most ~ 48 gr of water in the pore-space if we fully saturated the samples. Since we add less than 3 grams of water, this means that our experiments add water to about 5% of the pore-space. By estimating what the details of the pore-space look like, we can calculate two end-member states for the saturation of the sample. In both states, we make assumptions that are clearly not satisfied by our sample about the grains and pores; we thus give order-of-magnitude estimates. For the first case, we calculate how many layers of water molecules the introduced water corresponds to spread evenly throughout the pore space assuming a face-centered cubic (fcc) lattice of close-packed spheres. For the second case, we estimate how many pores we can fill completely with water.

[a)] Electronic mail: skt660@mun.ca; Also at Department of Physics and Physical Oceanography, Memorial University, St. John's, Newfoundland and Labrador, Canada, A1B 3X7
[b)] Also at Department of Earth Sciences, Memorial University of Newfoundland, St. John's, Newfoundland and Labrador, Canada, A1B 3X5

Porosity	$\phi =$ 0.05
Volume	$V_{total} =$ 956 cm^3
grain radius	$r = 2 \times 10^{-2}$ cm
Mass gain or loss	$m =$ 2.5 g
Thickness of a water molecule	$tw = 275 \times 10^{-10}$ cm
Density of water	$\rho =$ 1 g/cm^3

TABLE I. Table of sample properties and material constants.

For the first case, we make a rough estimate by assuming that we have monodisperse and spherical close-packed grains in an fcc arrangement. The numerical values of the various parameters are given in Table I. Using an fcc unit cell, we compute the surface area of the pores within the cell and then the number of cells we would need to fill our sample. This allows us to put an upper bound on how many layers of water molecules would make a uniform covering of the pore space. We estimate this to be approximately 10^3 molecules.

The necessary calculations are quite straightforward. We first calculate the total volume of pores

$$V_{pore} = V_{total} \times \phi \approx 48 \text{ cm}^3$$

and then the total volume of water

$$V_{water} = \frac{m}{\rho} = 2.5 \text{ cm}^3.$$

We then compute the percentage of the total pore space that can be filled with water, given the observed mass change

$$\frac{V_{water}}{V_{pore}} \times 100 \approx 5\%.$$

Estimating the surface-area of the pore space is slightly more involved and requires us to assume some sort of grain packing. As mentioned above, we use fcc packing as it results in the smallest porosity of the standard models. We then work with a standard fcc unit cell, which contains a total of 4 spheres[?] . The volume of a unit cube in an fcc lattice is

$$V_{fcc} = (4r/\sqrt{2})^3 = 2 \times 10^{-4}.$$

We then compute the number of fcc unit cubes in our sample:

$$n_{fcc} = V_{total}/V_{fcc} \approx 5 \times 10^6,$$

and the total surface area of the pores in our sample:

$$S_{total} = n_{fcc} \times S_{fcc} = n_{fcc} \times 4 \times (4\pi r^2) \approx 1 \times 10^5 \text{ cm}^2,$$

where we have simply calculated the surface area of the four spheres within the fcc unit cell. We can now compute the thickness of the water layer on our pores by

$$w_{thick} = V_{water}/S_{total} \approx 2.5 \times 10^{-5} \text{ cm}.$$

We then calculate the total number of water molecules:

$$n_{water} \approx w_{thick}/tw \approx 10^3.$$

For the other end-member calculation, we simply note that if all of the porosity were contained in equal-sized pores, then approximately 5% of those pores would be filled with water since 5% of the total pore volume is filled with water in our experiments.

[1] A. Dorfmann and R. W. Ogden, "Electroelastic waves in a finitely deformed electroactive material," IMA Journal of Applied Mathematics **75**, 603–636 (2010).